INTERANNUAL AND ANNUAL VARIATIONS IN THE GEOPOTENTIAL OBSERVED USING SLR

C.M. Cox(1,2), B. F. Chao(2), and A. Au(1,2)
(1) Raytheon Information Solutions, Landover, Maryland, USA
(2) Space Geodesy Branch, NASA Goddard Space Flight Center

Abstract

Recent Satellite Laser Ranging derived long wavelength gravity time series analysis has focused to a large extent on the effects of the recent large changes in the Earth's zonals, particularly J_2, and the potential causes, or the long-term secular rates. However, it is also possible to estimate the shorter wavelength coefficients, including non-zonals, over monthly time scales, and to connect these with known geophysical signals. For example, the results of Cox and Chao [2002] showed that the recovered J_3 time series shows remarkable agreement with NCEP-derived estimates of atmospheric gravity variations. Likewise, the non-zonal degree-2 terms showed reasonable correlation with atmospheric signals, as well as climatic effects such as El Niño Southern Oscillation. While the formal uncertainty of these terms is significantly higher than that for J_2, it is clear that there is useful signal to be extracted. Consequently, the SLR time series has been reprocessed to improve the time variable gravity field recovery, with the intent of recovering complete fields through maximum spherical harmonic degree 4. Initial comparisons of the average annual signals with the GRACE monthly fields shows a promising agreement over the continents, The recovered gravity rate map also is in general agreement with expectations of post-glacial rebound, depending on the period considered. We will present recent updates on the J_2 evolution, as well the interannual and annual variations of the gravity field, complete through degree 4, and geophysical and climatic connections.

Introduction

The long time history of satellite laser ranging (SLR) provides an absolutely unique data set of observations for the analysis of geophysical changes. Analysis of SLR tracking has yielded precise determination of the temporal variation in the low-degree spherical-harmonic components of Earth's gravity field, beginning with the initial observations of J_2 change made by observing Lagoes-1 orbital node accelerations [*Yoder et al*., 1983; *Rubincam*, 1984]. Those earliest results demonstrated the ability to observe large-scale terrestrial change using SLR. More recent studies have extended the knowledge to higher degree zonals [e.g. *Gegout and Cazenave*, 1993; *Cheng et al*., 1997; *Cox et al.,* 2003], and examined the annual signals in the low-degree geopotential, the non-tidal part of which is dominated by climatological signals. Overall, SLR data have played a key role in understanding changes in the solid Earth at millennial and decadal time scales, as well as providing insight into climatological variations over annual time-scales.

Analysis of the J_2 signal

Figure 1 shows the complete J_2 data series. With the exception of the additional data, it is similar to Figure 1 of *Cox and Chao* [2002]. Processing and development of the series is described in

Cox et al. [2003]. The 1998 J_2 anomaly is evident as the hump after that period. It is also characterized by a change in the amplitude and nature of the seasonal cycle. The anomaly appears to start earlier than 1998, however, that portion of the departure from the long-term trend is the result of atmospheric mass variation. This is shown in Figure 2, which compares the J_2 series after removal of the pre-1998 slope and annual signals, with that based on NCEP-derived atmospheric mass signal. After sometime in 2001, it appears as if the anomaly has changed slope, returning to something closer to the expected signal, however, it has not recovered to the original path that the pre-1998 slope would predict.

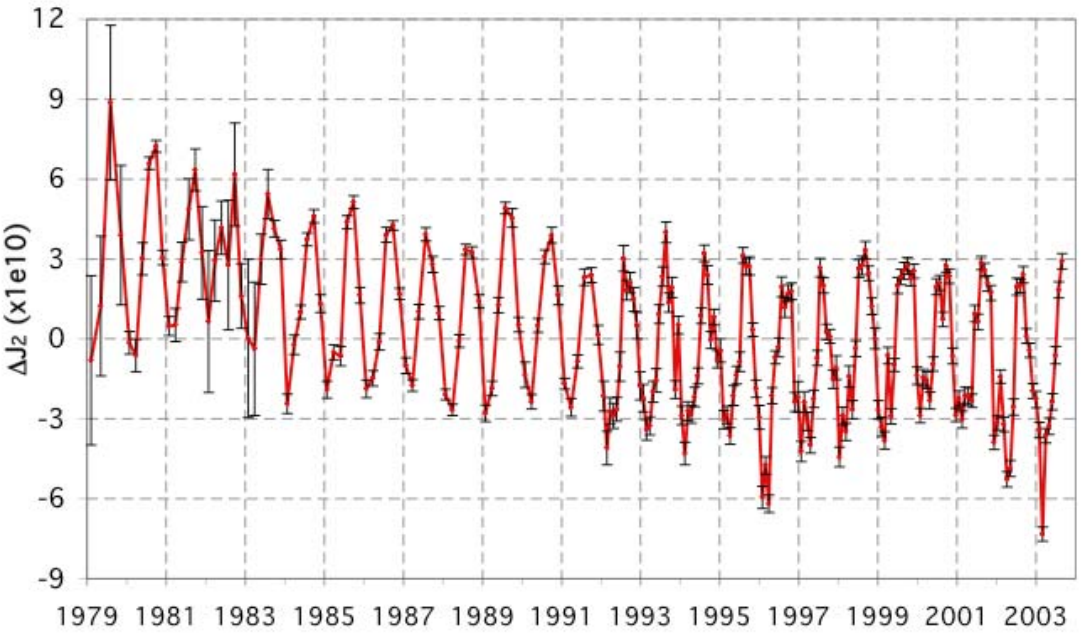

Figure 1. Observed ΔJ_2, including the atmospheric signal. Error bars are the observed J_2, uncertainties.

In addition to the J_2 zonal, time series for J_3 was also estimated. The J_3 zonal, which describes north-south mass distribution, does not show any significant anomalies corresponding to the timing of the J_2 anomaly. Provided this result is accurate, it implies that whatever is causing the J_2 anomaly is largely symmetric around the Equator.

The cause of the anomaly has not been positively identified, however, it has been associated with oceanic [*Chao et al.* 2003] and possible glacier mass changes [*Dickey et al.*, 2002]. The timing of the J_2 anomaly onset corresponds to the last big El Niño event, raising the possibility of an oceanographic connection. If the TOPEX/Poseidon (T/P) sea surface height (SSH) data is treated as being entirely caused by mass redistribution, the implied change in J_2 is consistent with the SLR results, if not a close match. EOF/PC (Empirical Orthogonal Function/Principal Component) analysis of the sea surface temperature (SST) and T/P SSH for the extratropic Pacific regions show an abrupt change around 1998. A breakdown of the SSH analysis for each region (not shown) indicates that the Northern pacific is the dominant contributor. The SST mode corresponds to the Pacific Decadal Oscillation (PDO), which is correlated at some level

with the observed J_2 data [*Cazenave and Nerem*, 2002]. Figure 3 shows the J_2 series compared with the SST-derived PDO Index. The correlation implies a connection with that ocean mode.

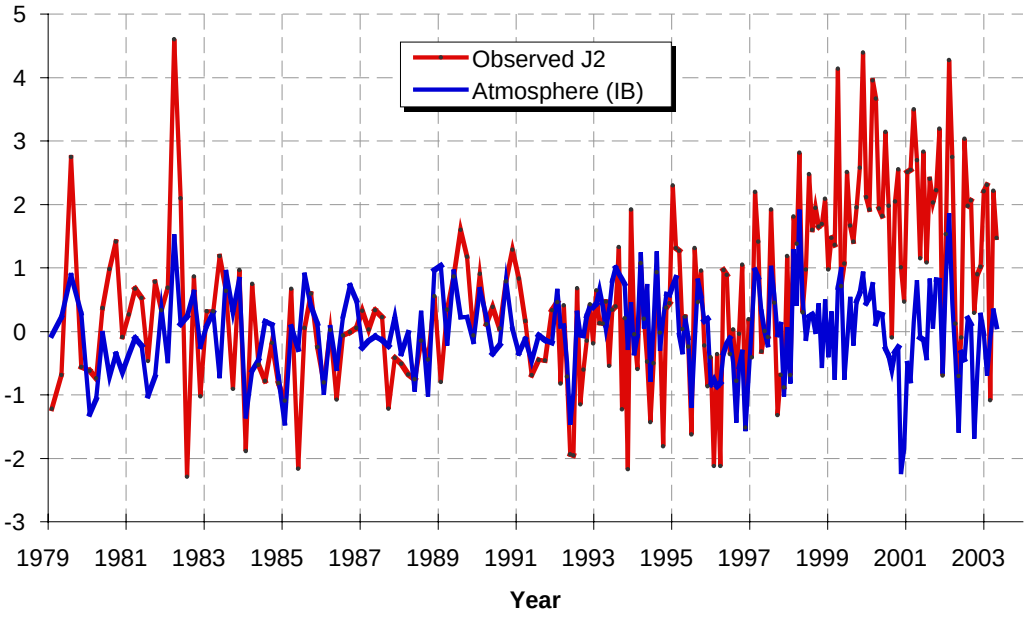

Figure 2. Observed ΔJ_2, after removal of pre-1998 slope and annual signals, compared with the corresponding atmospheric time series.

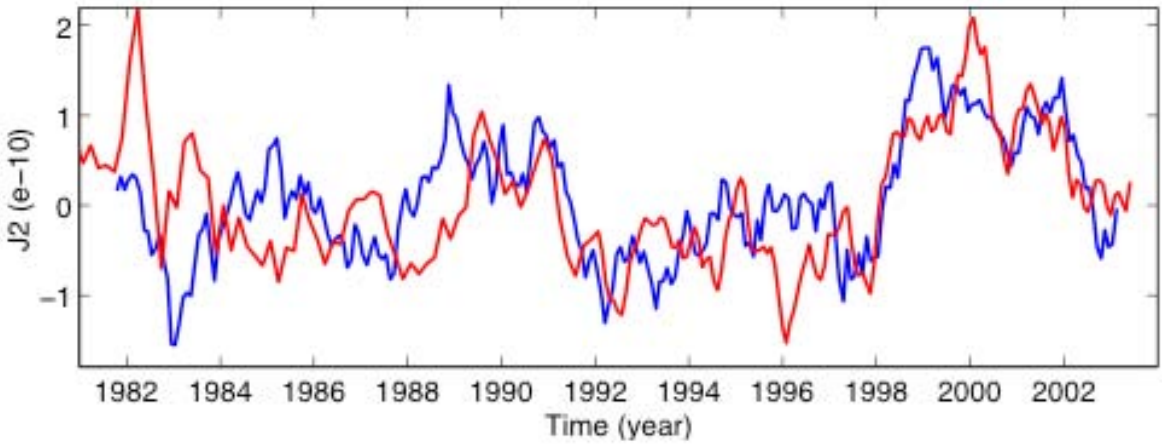

Figure 3. Non-seasonal ΔJ_2 (red curve) and the Pacific Decadal Oscillation (PDO, blue curve). The pre-1998 slope was removed from the ΔJ_2 series, as well as all annual signals. The PDO Index time series has been shifted to the right by five months.

Figure 4 shows a comparison of the atmosphere corrected J_2 series, after removal of the background (pre-1998) slope, with the cumulative totals from hydrology, the ocean, and sub-polar glaciers. The curve shown in green is the NCEP-derived soil hydrology. It shows some similarities, including the pre-anomaly dip, and a rise during the anomaly, but at most explains 20% of the anomaly. The blue curve shows the combination of the hydrology signal with the results from the assimilation mode output of the ECCO consortium ocean model [*Stammer, et*

al., 1999] as run by JPL (run KF047A). The ocean may explain another 20% of the anomaly. The results of *Cox and Chao* [2002] dismissed sub-polar glaciers as a primary cause of the anomaly based on the estimated mass flux data then available for the period up through 1998. *Dickey et al.* [2002] pointed out scenarios where the glacier contribution could be a possible major contributor (in addition to the oceans) based on three extrapolations of the glacier data. The black curve in figure 3 shows the total of the hydrology, ocean, and sub-polar glacier data using updates to the observations complete through 2001 [*Dyurgerov*, 2005]. The sub-polar glaciers may contribute another 20% to the total. Overall, the three geophysical signals only explain no more than half of the 1998 J_2 anomaly.

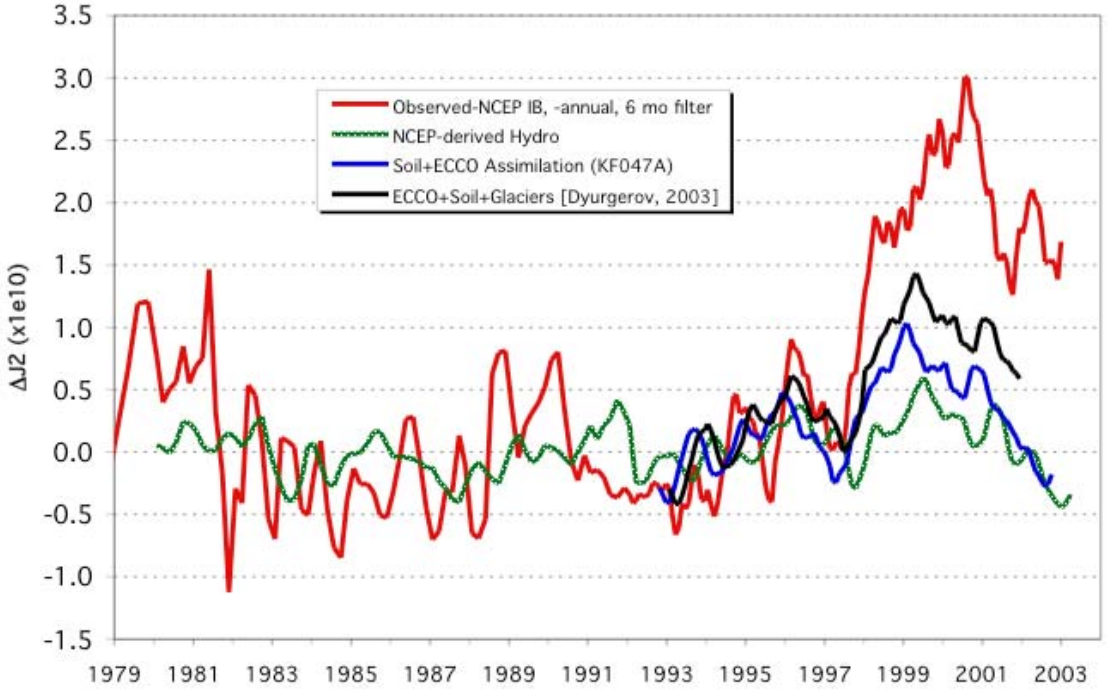

Figure 4. Non-seasonal atmosphere-corrected ΔJ_2, and the modeled contributions of hydrology, the oceans (ECCO Assimilation run KF047A), and estimated mass changes in the sub-polar glaciers.

The insufficiency of the hydrology, ocean, and glacier variations to explain the J_2 anomaly should not be unexpected. These represent only three potential contributors, and for that matter the models used to represent them are not complete. Greenland and Antarctica, which are not included in the glacier statistics, may have contributing roles. In addition the polar seas, which are not modeled in ECCO, and the actual hydrological signal including aquifers may have contributions. Furthermore, the oceanic global circulation models tend to underestimate the true variabilities.

All of the signals investigated to explain the J_2 anomaly have regional components that are non-zonal in nature, which may be useful for positive identification of the contributors to the J_2 anomaly. Comparison of the geophysical models with an appropriate observed gravity time series will allow identification of the known contributors to the interannual variations, as well as

identify gaps in our knowledge of global mass transport. The earlier results of *Cox and Chao* [2002] were primarily designed to recover zonal signals -- while there is some non–zonal signal of interest in the available series [*Cox et al*., 2003], the longitudinal signals have been suppressed for the most part.

Revised Processing

In an effort to recover a complete time-variable gravity time series, a new series has been prepared that is complete through spherical harmonic degree 4 from 1976 through 2004. The series was estimated at 60-day intervals prior to 1993, and nominally 30-day (actually 3 T/P cycles) after that point. This series used SLR tracking of Lageos-1, Lageos-2, Starlette, Ajisai, Stella, Westpac, and limited amounts of SLR and DORIS tracking of T/P. The ITRF2000 reference frame was used with the latest NASA GSFC pre-GRACE gravity field model - pgs7751q2 – which was a development of EGM96 [*Lemoine et al*., 1998]. The solid Earth tides are modeled in the same fashion as EGM96. Monthly atmospheric time-variable gravity complete through spherical harmonic degree 5, and with respect to the mean for 2000-2001, were made based on the NCEP monthly pressure fields, and the assumption of an inverse barometer (IB) response over the oceans. The GOT99 ocean tide model [*Ray*, 1999] was used in a "Demos number" representation [*Christoldoulidis et al*., 1988] with equilibrium values for Sa and Ssa C_{20} tides, and zero for the other harmonics of those tides. The tide model was complete through degree 10 for the following constituents: 2N2, 2Q1, Ae2, J1, L2, M1, Oo1, Phi1, Pi1, Psi1, R2, and T2. A number of the constituents were modeled to degree 20: K1, K2, M2, N2, O1, P1, Q1, S2. The 18.6-year and 9.3-year ocean tide C_{20} amplitudes were set to the values estimated in a comprehensive solution using data from 1979 through 1997 [*Cox et al.*, 2002]. Rates and annuals for the $C_{2...4,0}$ zonals derived from the earlier processing were used in the data reductions and gravity solutions, then restored in the post processing.

Interannual signals

The revised C_{20} time series is shown in Figure 5. The signal is generally commensurate with the previous J_2 ($=-\sqrt{5}C_{2,0}$) time series, although there is a new feature in the 1984-1986 period, which also appears in C_{40} series (Figure 6). There is some correlation with the C_{40} signal suspected in this case (overall correlation between the two series only 0.4). Post-1998 both the C_{20} and C_{40} series show significant anomalies. In this case correlation between the two series is not suspected, due to more satellites being present in the solution, and the fact that if it is spatially driven correlation in both the 1984 period and the post-1998 period, the correlation should have a consistent sign.

Because of concerns over possible correlations, the average geoid height by latitude band was computed, looking at the equatorial region (|lat|<30°), mid latitudes (30°< |lat| < 60°) and polar regions (60°<|lat|). The results are shown in Figure 7. As the figure shows, the mid-latitude geoid has remained fairly constant over the entire period. However, around 1996 to 1998, the polar geoid started to drop, whereas the equatorial geoid rose. This is indicative of a mass transport from the high latitudes to the low latitudes of large proportion, as it must overcome post-glacial rebound (see next section) to result in such a drop in the polar geoid [*Cox and Chao*, 2002].

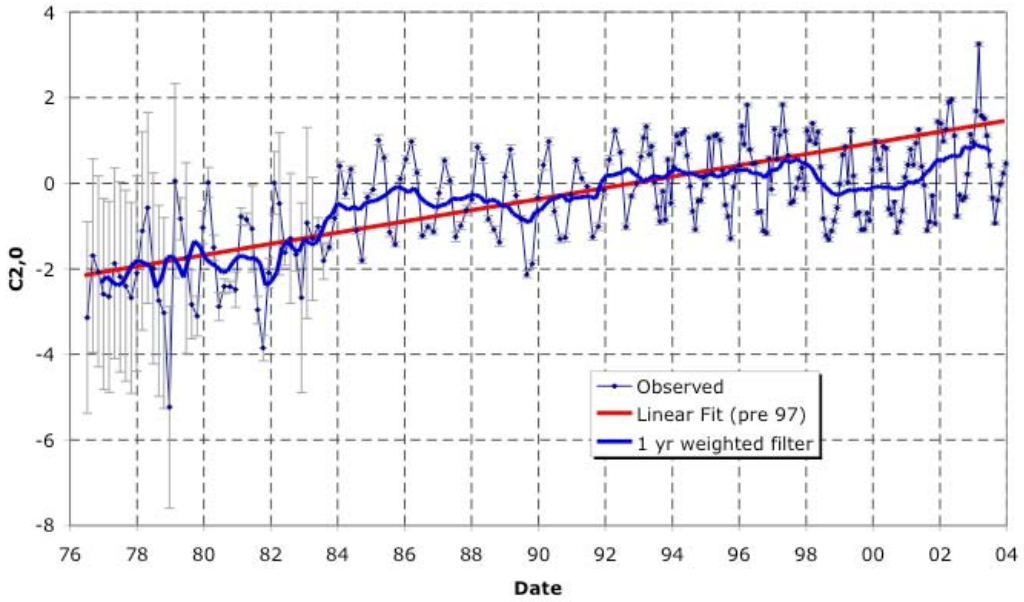

Figure 5. C_{20} from revised processing. Units are $1x10^{-10}$

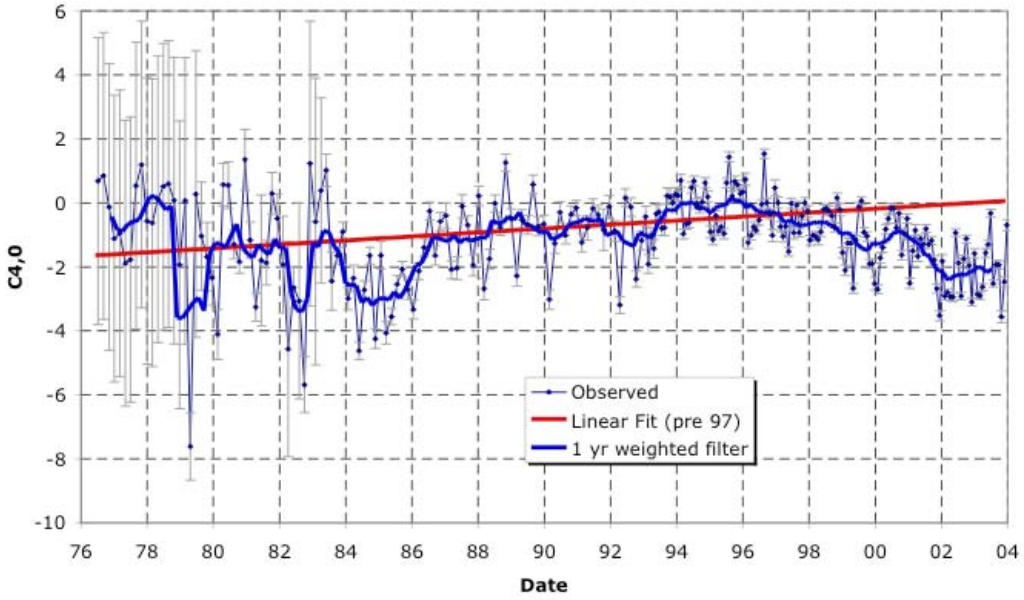

Figure 6. C_{40} from revised processing. Units are $1x10^{-10}$

The non-zonal terms of the gravity also show significant changes. Figure 8 shows the time series for the S_{33} term, which is dependent only on longitude. This spherical harmonic coefficient shows some of the larger signals. Significant variation is seen in the 1986-1992 period, but this period is determined with only three satellites (Starlette, Ajisai, and Lageos1), so it could be satellite related. After 1993 there are several more spacecraft involved and the variations are smaller. However, after 2000 there are substantial departures that are of the magnitude seen with the zonals.

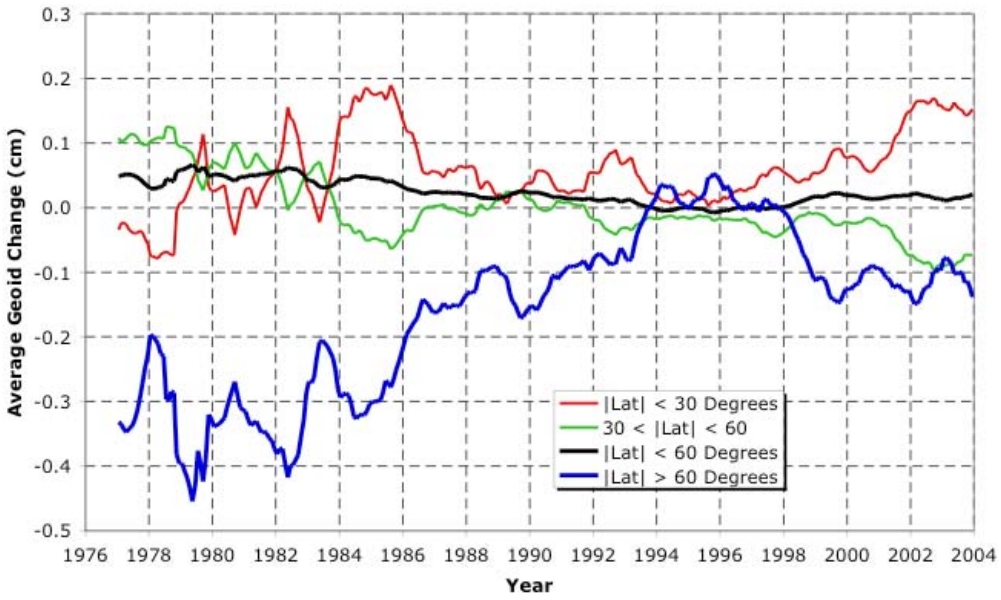

Figure 7. Zonal changes in the geoid over the equatorial (|lat|<30°), mid latitude (30°< |lat| < 60°) and polar regions (60°<|lat|). An annual filter has been applied to the data.

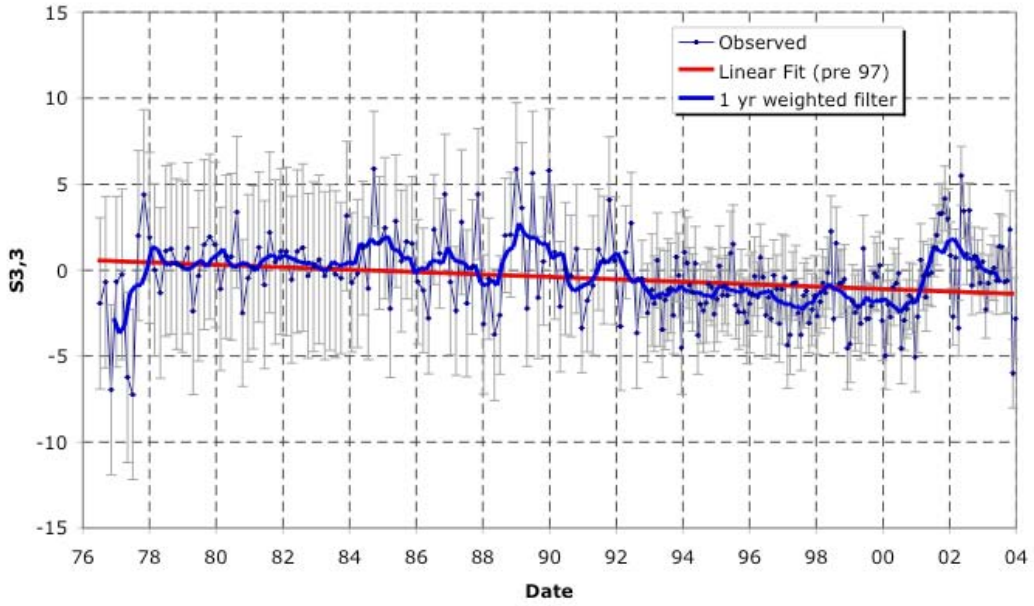

Figure 8. S_{33} from revised processing. Units are $1x10^{-10}$.

Geoid Rates

As discussed earlier, SLR has been used to assess zonal changes in the gravity field, but it has not been used to directly assess the changes in the complete geoid. Preliminary geoid rates complete through degree 4 have been computed from the time series, and are shown in the map Figure 9 for the 1980-1997 period. The rates shown are with respect to the IERS2000 definition for the C/S_{21} rates. For this computation, the post-930101 SLR solution data was effectively weighted at 2x the earlier data. For the period 1980-1997 there are large increases in the Greenland/North America and Antarctic regions (~0.5 mm/yr). For comparison, Figure 10 shows the corresponding geoid rate amp through degree 4 due to the mantle post-glacial rebound (PGR), computed by Erik Ivins (see http://bowie.gsfc.nasa.gov/ggfc/mantle.htm), based on an ICE-3G ice loading history model and a lower mantle viscosity of $2x10^{21}$ Pa s. As that model shows, the principle features at the 5000 km spatial scale of the SLR results is confined to the Hudson Bay area and Greenland in the northern hemisphere, and a fairly uniform, and larger, change over the south pole. There are some features at the lower latitudes, but they are much smaller, relative to the polar changes, than those seen in the SLR results. For the full period over 1980-2002 the observed geoid change is reduced by 50% (Figure 11). Of note is the relative scale of the changes over Greenland and Antarctica, with Greenland dominating, which is reversed from that expected based on PGR. Either present-day mass loss in Antarctica, or less likely, mass accumulation in Greenland could explain this feature.

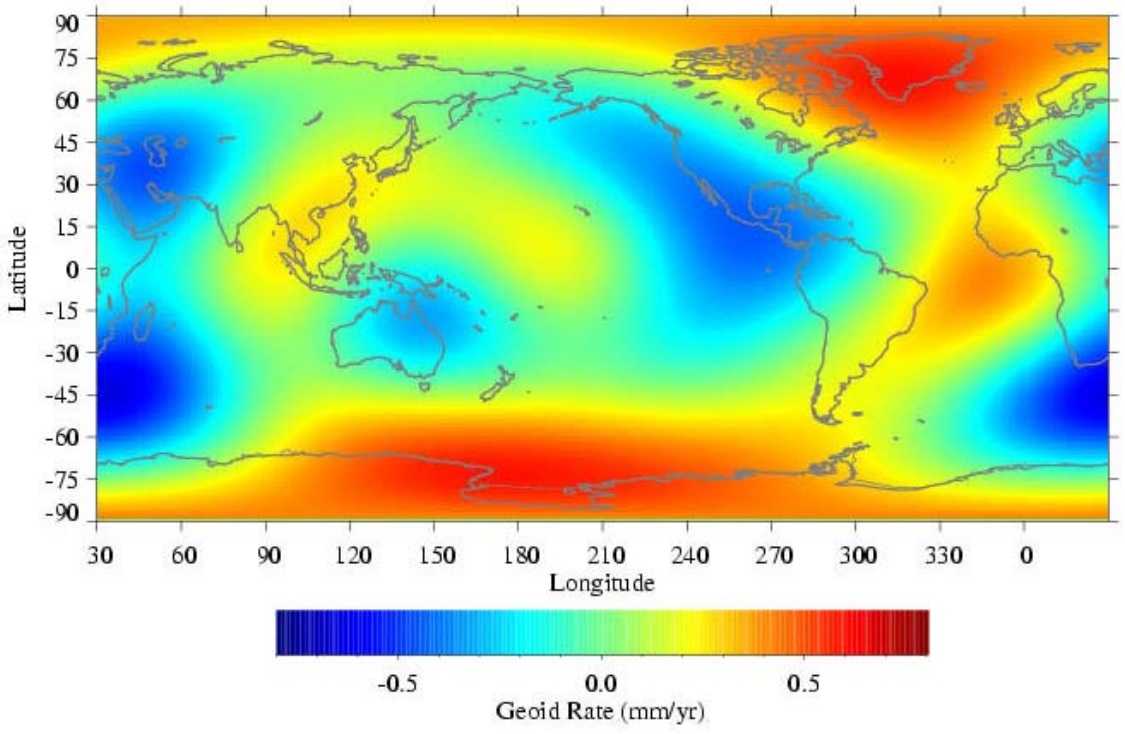

Figure 9. Mean geoid rate map in mm/yr derived from SLR tracking from 1980 through 1997. shown with respect to the IERS definition for the C/S_{21} rates.

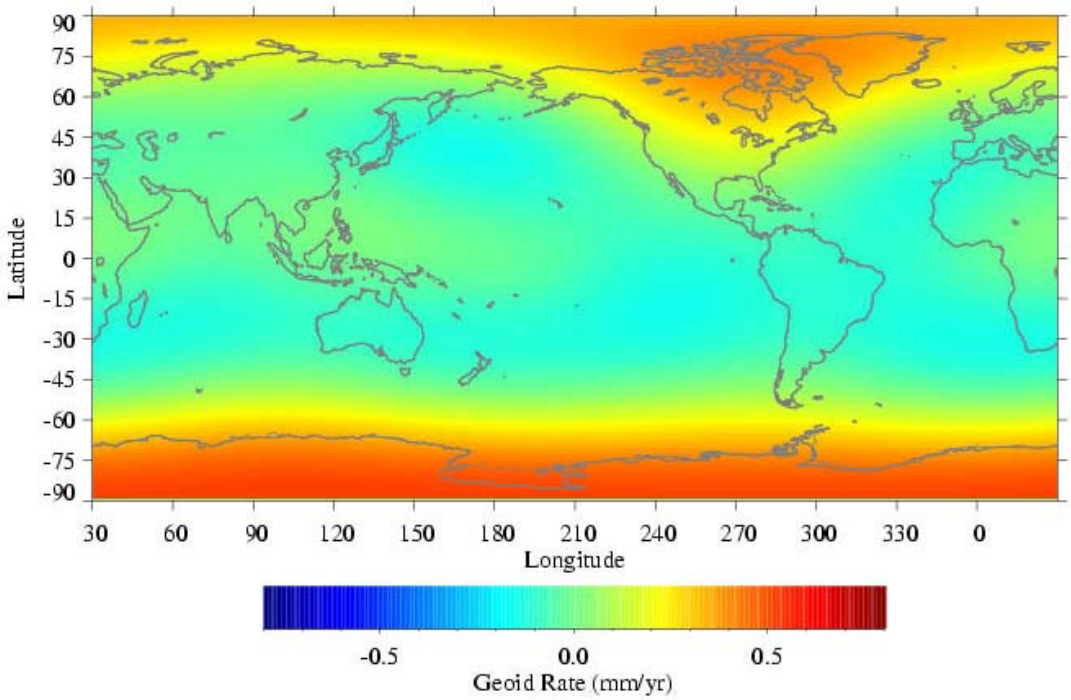

Figure 10. Mean geoid rate map for PGR in mm/yr through degree 4, predicted based on an ICE-3G ice loading history model and a lower mantle viscosity of $2x10^{21}$ Pa s (courtesy of Erik Ivins).

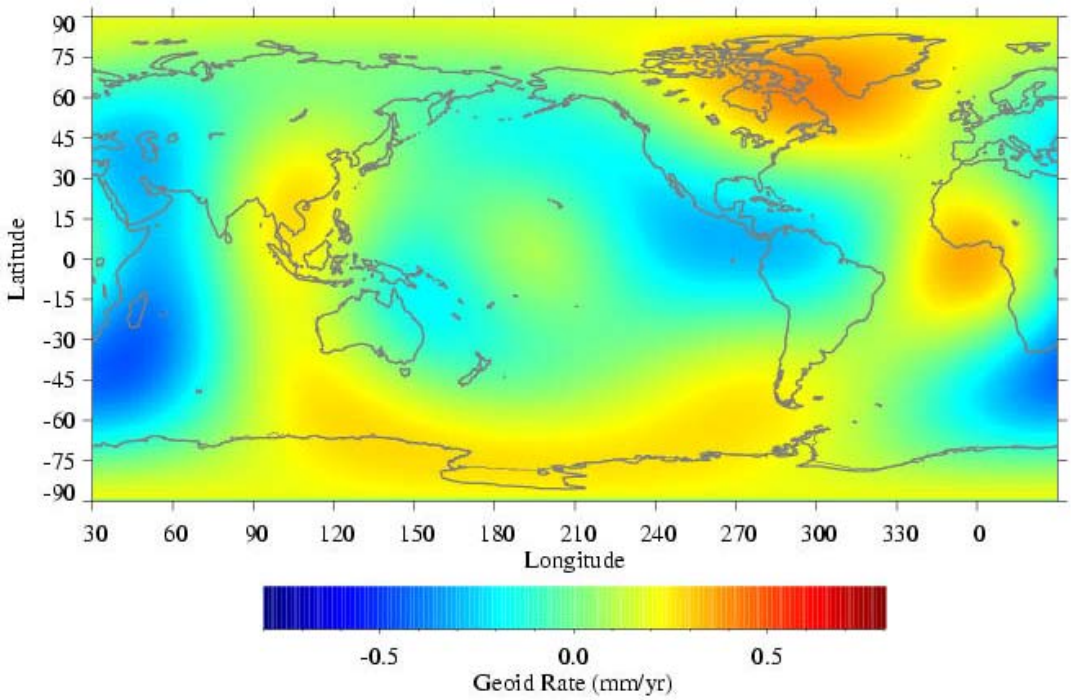

Figure 11. Same as Figure 9, but for the period 1980 through 2002.

The comparatively large changes sensed by SLR in the low latitude regions are commensurate with the T/P observed sea-level change shown in Figure 12 [Figure 3 from *Anderson et al*., 2002]. Both show prominent increases in the western Pacific and a drop in the eastern Pacific, as well as a general increase in the Atlantic. The implication is that the sea level changes represent actual mass transport, and that the changes in sea level are not the sole result of steric effects by themselves.

More detailed analysis is required, including: error assessment, consideration of steric effects for the ocean data comparisons, and comparison with hydrological changes over land in order to make a more thorough assessment of the mass transport budgets. Nonetheless, the results shown here, although preliminary and qualitative in nature demonstrate that SLR may have merit in looking at climate induced mass transport at the decadal scales.

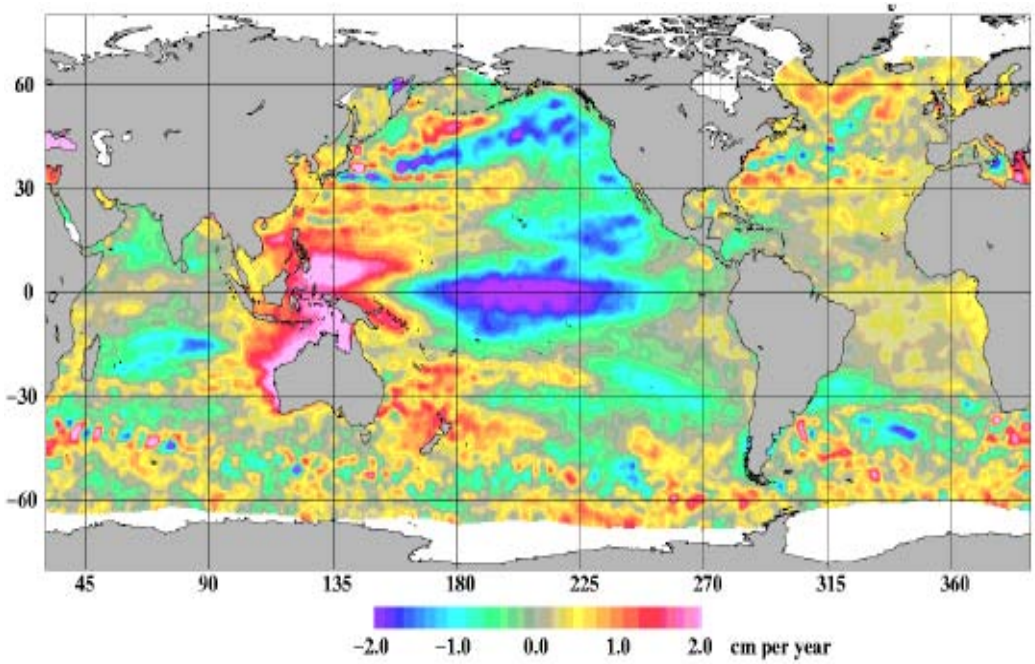

Figure 12. Sea Level trend from T/P for the period from September 1992, through February 2000. From figure 3 in *Anderson et al*., [2002].

Annual and Semi-Annual Signals

In contrast to the large differences between the SLR and GRACE time-variable gravity fields, similar seasonal (annual and semi-annual) variations are present in both. Figure 13 shows the monthly sequence maps, complete through degree 4, expressed as the equivalent water height [e.g., *Chao*, 2005]. The SLR seasonal terms were derived from the 5-year period 1998-2002. The nineteen GRACE (UT/CSR) monthly solutions were fit with mean, linear, annual, and semi-annual terms, and only the annual and semi-annual terms plotted.

There are some significant differences in the make up of the fields. First, the treatment of the ocean correction is different. The SLR series only considers the IB response to the atmosphere,

whereas the GRACE products are corrected for both pressure and wind driven changes in the ocean mass distribution based on a barotropic ocean model [*Tapley et al*., 2004]. The C_{20} annual and semi-annual terms from both data sets were used in generating the maps, however a large rate was removed from the GRACE data. Also, in an attempt to match the nature of the $C_{odd,0}$ term estimated in the SLR results, the C_{30} and C_{50} GRACE terms were used. Finally, the selected time periods differ, making the comparison valid only in terms of the "average" signal, and then only in the case where climate variability does not cause changes in the amplitude, and possibly phase, of the variations. There is some indication of this in the long C_{20} time series (not shown).

Despite the differences in the make up of the solutions, the seasonal signals have fairly good agreement over land. The seasonal cycle over the Amazon (peaking in April/May) is captured by both SLR and GRACE datasets. There are similar structures and evolutions over Africa and Europe as highs and lows move from East Africa to Northwest Africa to the North Atlantic then to Europe, and east into Asia. Also, the monsoons in India, peaking in July/August, then progressing east and north along the Asian coast, are evident in both sets of results. The SLR results do show more power over the oceans, which is expected since only the IB (not the wind-driven) ocean correction was applied. Likewise, there are differences in the polar latitudes, possibly caused by the differences between $C_{odd,0}$ from SLR and C_{30} +C_{50} from GRACE.

Conclusions

A large anomaly in C_{20} (or J_2) began sometime around 1998, and has persisted until the present time. Sometime in 2001, the slope changed again. The C_{20} signal has returned about 50% of the way to the long-term trend dictated by PGR. Consequently, the deviation may be interannual in nature, and therefore does not necessarily represent a departure from the long-term trend. Overall the signal is well correlated with the pacific decadal oscillation, however the available ocean data does not explain the mass anomaly. The oceans, continental hydrology, and sub-polar mountain glaciers may each explain ~20% of the anomaly.

The revised processing, intended to recover complete gravity fields, has resulted in more signal in the C_{30} and C_{40} series. While there is some concern over their separability, the sum of the zonal terms $C_{2..4,0}$ terms indicates the possibility of a rapid drop in the geoid over the polar regions. There is a corresponding rise in the geoid in the lower latitudes, but as of yet ascertaining where the presumed ice mass went (ocean or land) is not possible.

The observed geoid rates are similar to the PRG predictions. The signal in the northern regions is larger compared to the Antarctic regions than the PGR models predict. Is the excess related to present-day mass loss? There are also differences in the Equatorial regions, with more rise being observed in the Atlantic than is predicted by the PGR models. The rise is in general qualitative agreement with the observed sea level trend.

There is reasonable agreement between the annual and semi-annual time-variable gravity signals derived from 5 years of SLR observations, and the 19 monthly solutions available from the GRACE Mission at spatial scales of ~5000 km. However, there are significant differences in the mean fields and individual spherical-harmonic terms estimated at monthly timescales.

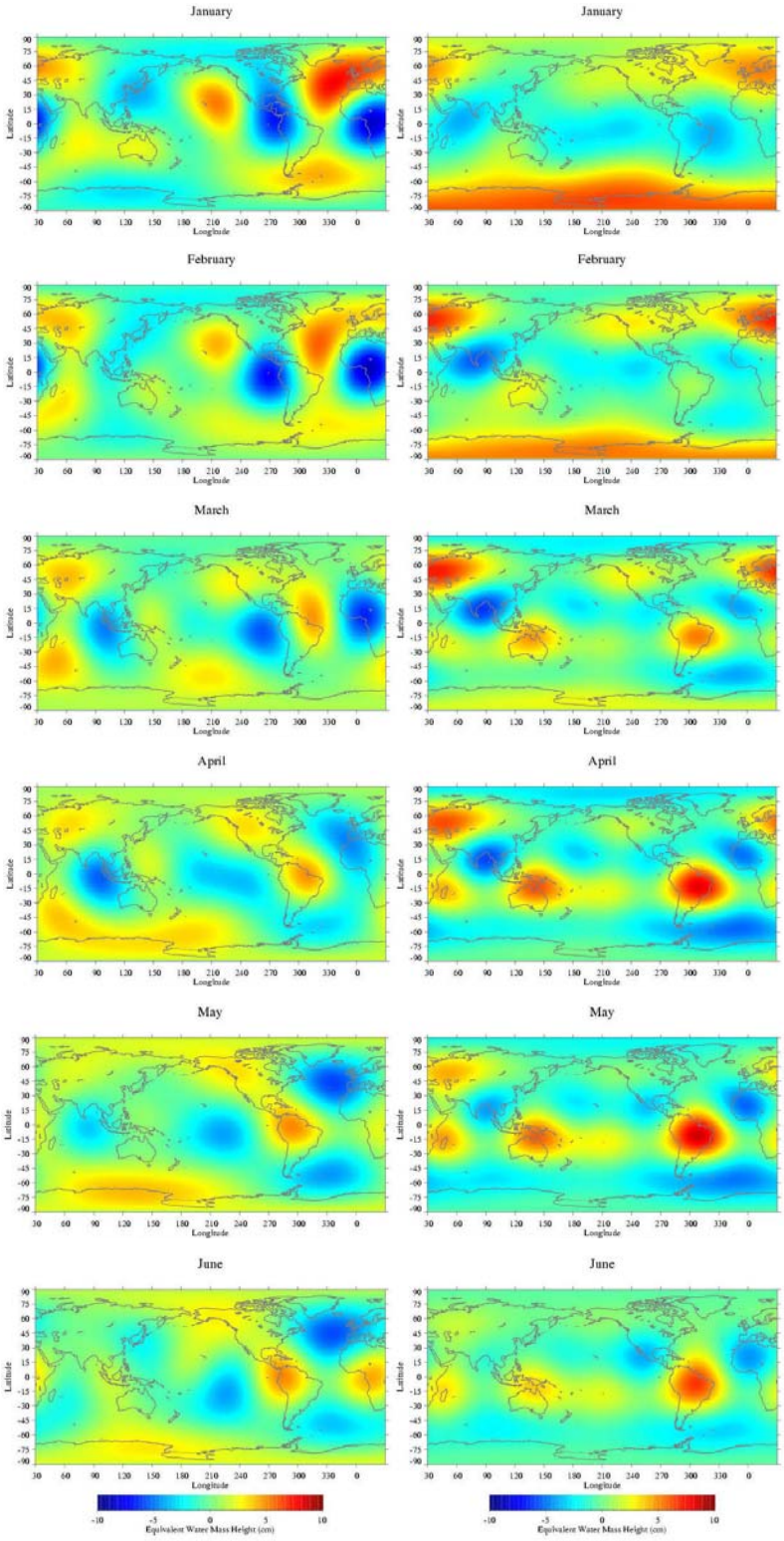

Figure 13a. Seasonal (annual plus semi-annual) time-variable gravity field expressed in terms of equivalent water height, January (top) through June (bottom). The SLR/DORIS results are shown on the left and the GRACE on the right. The color scale range is ±10 cm.

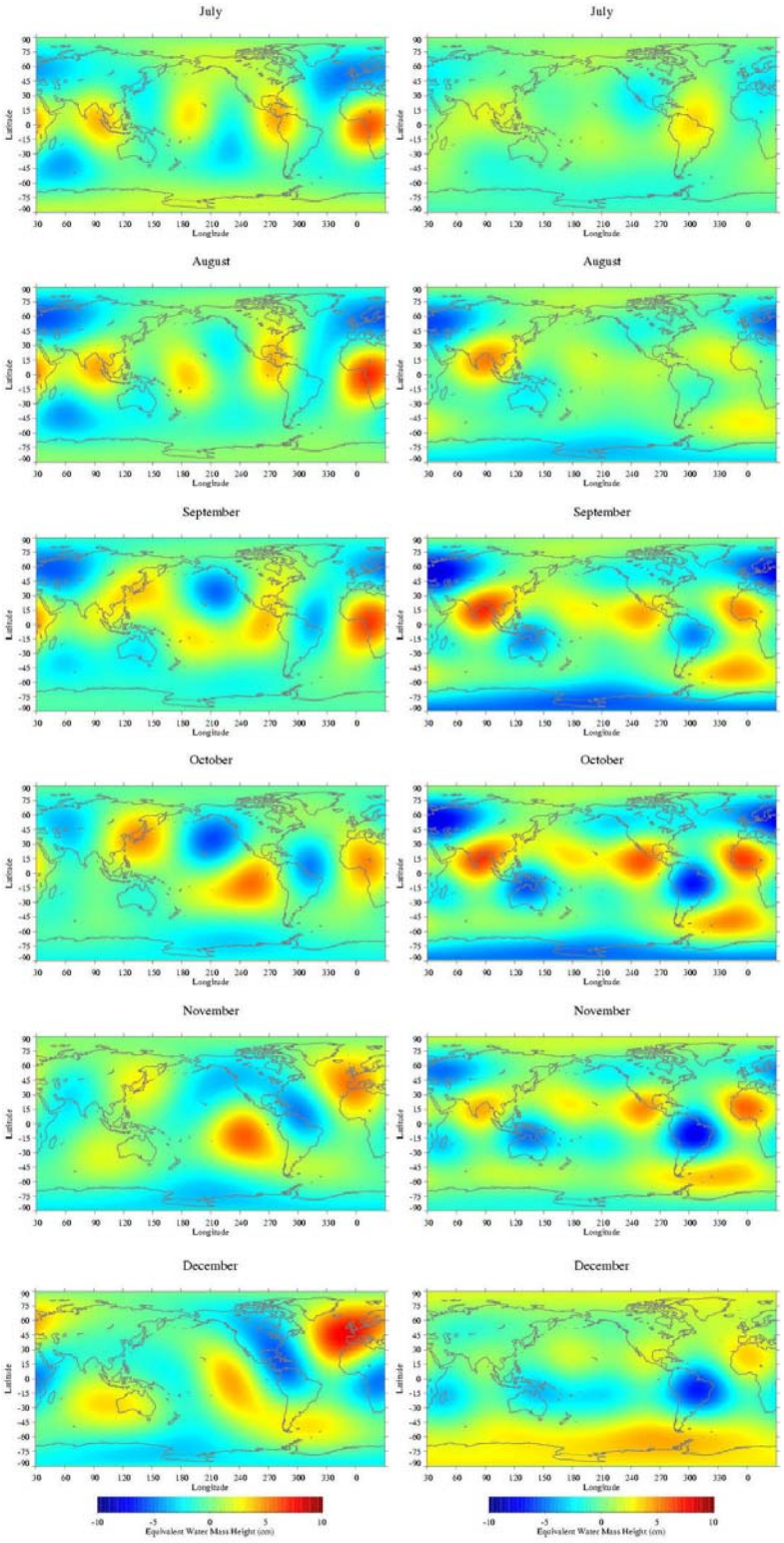

Figure 13b. Seasonal (annual plus semi-annual) time-variable gravity field expressed in terms of equivalent water height, July (top) through January (bottom). The SLR/DORIS results are shown on the left and the GRACE on the right. The color scale range is ±10 cm.

References

Anderson, O.B., P. Knudson, and B. Beckley, Monitoring Sea Level and Sea Surface Temperature Trends from ERS Satellites, *Phys and Chem of the Earth*, 27, Nos 32-34, 1413-1418, 2002.

Cazenave, A., and R.S. Nerem, Redistributing the Earth's Mass, 297, 783, August 2, 2002.

Chao, B. F., On inversion for mass distribution from global (time-variable) gravity field, in press, *J. Geodynamics*, 2005.

Cheng, M.K., C.K. Shum, B.D. Tapley, Determination of long-term changes in the Earth's gravity field, *J. Geophys Res*, **102**, 22377, 1997.

Christoldoulidis, D.C., D.E. Smith, R.G. Williamson, and S.M. Klosko, "Observed Tidal Braking in the Earth/Moon/Sun System," *J. Geophys. Res*., 93, B6, 6216-6236, 1988.

Cox, C.M., and B.F. Chao, Detection of a Large-Scale Mass Redistribution in the Terrestrial System Since 1998, Science, 297, 831, August 2, 2002.

Cox, C.M., A. Au, J.-P. Boy, and B.F. Chao, Time-Variable Gravity: Using Satellite-Laser-Ranging as a Tool for Observing Long-Term Changes in the Earth System, Proceedings of the 13th International Workshop on Laser Ranging, R. Noomen, S. Klosko, C. Noll, and M. Pearlman, eds., October, 2003.

Dickey, J. O., S. Marcus, O. de Viron, I. Fukumori, Recent Earth oblateness variations: Unraveling climate and postglacial rebound effects, *Science 298*, 1975-1977, 2002.

Dyurgerov, Mark. Glacier Mass Balance and Regime: Data of Measurements and Analysis. INSTAAR Occasional Paper No. 55, ed. M. Meier and R. Armstrong. Boulder, CO: Institute of Arctic and Alpine Research, University of Colorado. Distributed by National Snow and Ice Data Center, Boulder, CO. 2002, updated 2005.

Gegout, P. and A. Cazenave, Temporal Variations of the Earth's Gravity Field for 1985-1989 from Lageos, *Geophys J Intl*, 114, 347-359, 1993.

Lemoine, F.G., Kenyon, S.C., Factor, J.K., Trimmer, R.G., Pavlis, N.K., Chinn, D.S., Cox, C.M., Klosko, S.M., Luthcke, S.B., Torrence, M.H., Wang, Y.M., Williamson, R.G., Pavlis, E.C., Rapp, R.H., and Olson, T.R., The Development of the Joint NASA GSFC and the National Imagery and Mapping Agency (NIMA) Geopotential Model EGM96, NASA TR 206861, 1998.

Ray, R.D., A global ocean tide model from Topex/Poseidon altimetry: GOT99.2, NASA Tech. Memo. 209478, Goddard Space Flight Center, 58 pp., 1999.

Rubincam, D.P., Postglacial Rebound Observed by Lageos and the Effective Viscosity of the Lower Mantle, *J. Geophys Res*, 89, 1077-1087, 1984.

Stammer, D. et al., The consortium for estimating the circulation and climate of the ocean (ECCO) -- Science goals and task plan, The ECCO Consortium, Report No.1, November 1999.

Tapley, B. D., S. Bettadpur, J. C. Ries, P. F. Thompson, and M. M. Watkins, GRACE measurements of mass variability in the Earth system, *Science, 305*, 503-505, 2004.

Yoder, C.F., J.G. Williams, J.O.Dickey, B.E. Schutz, R.J. Eanes, B.D. Tapley, Secular Variation of earth's gravitational harmonic J_2 coefficient from Lageos2 and non-tidal acceleration of earth rotation, *Nature*, 303 (5920): 757-762 (1983).